Molding direction constraints in structural optimization via a level-set method

Grégoire Allaire, François Jouve, Georgios Michailidis

Molding direction constraints in structural optimization via a level-set method

Grégoire Allaire, François Jouve and Georgios Michailidis

Abstract In the framework of structural optimization via a level-set method, we develop an approach to handle the directional molding constraint for cast parts. A novel molding condition is formulated and a penalization method is used to enforce the constraint. A first advantage of our new approach is that it does not require to start from a feasible initialization, but it guarantees the convergence to a castable shape. A second advantage is that our approach can incorporate thickness constraints too. We do not adress the optimization of the casting system, which is considered a priori defined. We show several 3d examples of compliance minimization in linearized elasticity under molding and minimal or maximal thickness constraints. We also compare our results with formulations already existing in the literature.

1 Introduction

The increasing number of publications on industrial applications of shape and topology optimization reflects the interest of engineers to introduce these techniques in the design process of mechanical structures. Especially in case of complicated problems, where mechanical intuition is very limited, shape and topology optimization can serve as a valuable tool both in order to obtain an optimized structure and to accelerate the design process.

Grégoire Allaire
Centre de Mathématiques Appliquées (CMAP), École Polytechnique, CNRS UMR 7641, Université Paris-Saclay, 91128 Palaiseau, France, e-mail: gregoire.allaire@polytechnique.fr

François Jouve
University Paris Diderot, Laboratoire J.L. Lions (UMR 7598), Paris, e-mail: jouve@ljll.univ-paris-diderot.fr

Georgios Michailidis
SIMaP-Université de Grenoble INPG, France, e-mail: michailidis@cmap.polytechnique.fr

Among the several methods that appeared in the literature, such as SIMP (Solid Isotropic Material with Penalization) method [14, 49, 16], the homogenization method [3, 13, 15], the phase field method [18, 41, 51, 17] or the Soft Kill Option [31, 23], the level-set method for shape and topology optimization [10, 11, 35, 38, 44] seems to fulfill industrial requirements in a satisfying way. Using a level-set function to describe implicitly the boundary of a shape [36, 37] allows topological changes to appear in an easy way, while the geometric nature of the method is a benefit for the study of problems where the position of the interface plays a significant role (stress constraints, thermal problems with flux across the boundary, etc.). The method is independent of the objective function under study [7, 12, 20, 21] and the ability to adapt the mesh on the boundary [5, 6, 45] alleviates possible numerical difficulties due to the "ersatz" material or to the discontinuity of the material properties.

Moreover, industrial design introduces significant constraints according to the fabrication method, the tooling limitations and the total cost that can be afforded. Some of them are essentially geometric constraints, related to a notion of local thickness. We have shown in our previous work [9] that thickness can be explicitly controlled using a level-set method, which constitutes a great advantage for the industrialization of the method. Such constraints are of great significance for cast parts, i.e. structures that are intended to be constructed by casting.

Casting [19] is the fabrication process where molten liquid is poured into a cavity formed by molds. The final structure is obtained after solidification of the liquid and removal of the molds. Thus, the structure should have such a shape, so that the construction and the removal of the molds is possible without destroying either the structure or the mold. This is called the "molding constraint". The casting process imposes further specifications of mechanical nature on the shape of the structure, mainly related to the solidification and filling process. In [32], we argued that such constraints can be translated, in the context of topology optimization, into geometrical constraints on the maximum and minimum allowable feature size, since the complete casting system (molding, solidification and filling system) is usually designed after the structural form definition.

According to the choice of shape and topology optimization algorithm, different ways have been proposed to handle the molding constraint. In the framework of the SIMP method, which is a density method, Zhou et al. [50] implemented a penalization scheme that favors higher densities at the lower part of the structure. Leiva et al. [29] have chosen to introduce directly the growth direction in the parametrization of the problem, while methods of topology control, such as connectivity and growth direction control, have been applied for the Soft Kill Option [24]. A complete review of these methods and a comparison of results of topology optimization with and without manufacturing constraints can be found in [25, 26].

In the framework of the level-set method, the only works on the topic -to our knowledge- are those of Xia et al. [46, 47]. In [46] the authors have proposed a molding condition on the design velocity, i.e. a modification of the descent direction that ensures the castability of the shape at each iteration, provided that the initial shape is also castable. In this work, the molding system is a priori defined. In [47]

the authors have added the optimization of the draw direction in the optimization problem. The same choice for the design velocity is done. Although the method allows those topological changes that do not come in conflict with castability, it is mentioned in [46] that the shape cannot expand orthogonally to the casting direction. This is a great disadvantage in case one wants to impose a minimum thickness contraint.

In the present paper, we introduce a new approach to handle the molding constraint in the framework of the level-set method for shape and topology optimization. A pointwise constraint is formulated using the signed distance function and a penalty functional is then constructed to turn the constraint into a global one. A shape derivative [2], [27], [33], [34], [39] is calculated for this new functional and a simple penalization method is applied which guarantees that the optimal shape is castable at convergence. A first advantage of our new approach is that it does not require to start from a feasible initialization. This is of course a key feature since, in many industrial problems, it is very hard to find out a feasible design to start with. A second advantage is that our approach can incorporate thickness constraints, contrary to the previous method in [46, 47].

The contents of our paper is as follows. Section 2 describes our model shape optimization problem. For simplicity we focus on compliance minimization with volume constraint: the main difficulty on which we shall focus is the addition of further molding and thickness constraints. Section 3 is a short review of the level-set method. Section 4 discusses the casting process while Section 5 introduces our new molding direction constraint. We also recall the approach of Xia et al. [46, 47], as well as the "uniform cross-section surface constraint" of Yamada et al. [48], which simplifies a lot the shape of the desired molds. Section 6 is devoted to the computation of the shape derivatives of these molding constraints. Finally Section 7 features our 3-d numerical results which are obtained in the finite element software SYSTUS of ESI-Group [40], which is well adapted to an industrial context. Our results were partially announced in [8].

2 Setting of the problem

Our goal is to optimize a shape $\Omega \subset \mathbb{R}^N$ ($N = 2$ or 3), a bounded domain occupied by a linear isotropic elastic material with Hooke's law A (a positive definite fourth-order tensor). Typically, the boundary of Ω is comprised of three disjoint parts, such that $\partial\Omega = \Gamma_D \cup \Gamma_N \cup \Gamma_0$, with Dirichlet boundary conditions on Γ_D, non-homogeneous Neumann boundary conditions on Γ_N and homogeneous Neumann boundary conditions on Γ_0. We introduce a working domain D (a bounded domain of $\mathbb{R}^N$) which contains all admissible shapes, that is $\Omega \subset D$. The volume and surface loads are given as two vector-valued functions defined on D, $f \in L^2(D)^N$ and $g \in H^1(D)^N$. The displacement field u is the unique solution in $H^1(\Omega)^N$ of the linearized elasticity system

$$\begin{cases} -\mathrm{div}\,(A\,e(u)) = f & \text{in } \Omega, \\ u = 0 & \text{on } \Gamma_D, \\ \big(A\,e(u)\big)n = g & \text{on } \Gamma_N, \\ \big(A\,e(u)\big)n = 0 & \text{on } \Gamma_0, \end{cases} \tag{1}$$

where $e(u)$ is the strain tensor, equal to the symmetrized gradient of u. A classical choice for the objective function $J(\Omega)$ to be minimized is the compliance (the work done by the loads). It reads

$$J(\Omega) = \int_\Omega f\cdot u\,dx + \int_{\Gamma_N} g\cdot u\,ds = \int_\Omega A\,e(u)\cdot e(u)\,dx. \tag{2}$$

A typical shape optimization problem is

$$\inf_{\Omega\in\mathscr{U}_{ad}} J(\Omega), \tag{3}$$

where $\mathscr{U}_{ad}$ is the set of admissible shapes. Imposing that all shapes belong to the working domain D and that they satisfy a volume constraint $0 < V < |D|$, a possible choice of admissible set is

$$\mathscr{U}_{ad} = \{\Omega \subset D \text{ such that } |\Omega| = V\}. \tag{4}$$

As it is well-known [2, 16], problem (3) may lack an optimal solution. Numerically, the non-existence of a minimizer of (3) is reflected by the fact that approximate numerical solutions are mesh dependent (the finer the mesh the more details or finer members in the solution). Classically, to obtain existence of optimal shapes, one needs to restrict further the admissible set $\mathscr{U}_{ad}$ by imposing additional geometrical, topological or smoothness constraints [2, 34, 39].

In order to find a descent direction for advecting the shape, we rely on the Hadamard method of shape differentiation, following the approach of Murat and Simon [34]. Starting from a smooth reference open set Ω, we consider domains of the type

$$\Omega_\theta = \big(Id+\theta\big)(\Omega),$$

with $\theta \in W^{1,\infty}(\mathbb{R}^N,\mathbb{R}^N)$. It is well known that, for sufficiently small θ, $(Id+\theta)$ is a diffeomorphism in $\mathbb{R}^N$.

Definition 1. The shape derivative of $J(\Omega)$ at Ω is defined as the Fréchet derivative in $W^{1,\infty}(\mathbb{R}^N,\mathbb{R}^N)$ at 0 of the application $\theta \to J\big((Id+\theta)(\Omega)\big)$, i.e.

$$J\big((Id+\theta)(\Omega)\big) = J(\Omega) + J'(\Omega)(\theta) + o(\theta) \quad \text{with} \quad \lim_{\theta\to 0} \frac{|o(\theta)|}{\|\theta\|} = 0\,,$$

where $J'(\Omega)$ is a continuous linear form on $W^{1,\infty}(\mathbb{R}^N,\mathbb{R}^N)$.

A classical result states that the shape derivative $J'(\Omega)(\theta)$ depends only on the normal trace $\theta\cdot n$ on the boundary $\partial\Omega$ [27], [34], [39]. We refer to [11] for various

examples of shapes derivatives in the elasticity setting, including that for compliance.

3 Level-set framework

3.1 Shape representation

We favor an Eulerian approach and use the level-set method [36] to capture the shape Ω on a fixed mesh. Then, the boundary of Ω is defined by means of a level set function ψ (see Figure 1) such that

$$\begin{cases} \psi(x) = 0 \Leftrightarrow x \in \partial\Omega \cap D, \\ \psi(x) < 0 \Leftrightarrow x \in \Omega, \\ \psi(x) > 0 \Leftrightarrow x \in \left(D \setminus \overline{\Omega}\right). \end{cases}$$

During the optimization process the shape is being advected with a scalar (normal) velocity $V(x)$ derived from shape differentiation, as we will see in the sequel. The advection is described in the level-set framework by introducing a pseudo-time $t \in \mathbb{R}^+$ and solving the well-known Hamilton-Jacobi equation

$$\frac{\partial \psi}{\partial t} + V|\nabla\psi| = 0. \tag{5}$$

using an explicit second order upwind scheme [37].

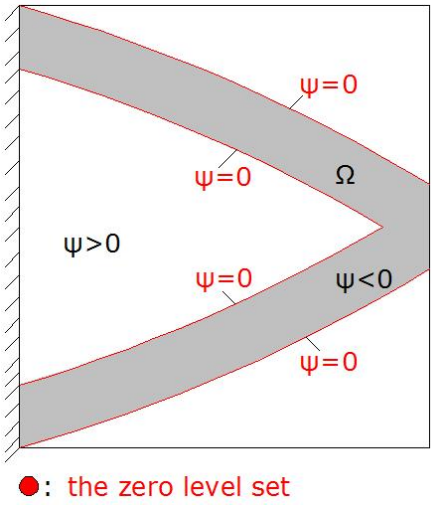

Fig. 1 Level-set representation of a shape.

3.2 Signed distance function

We recall that if $\Omega \subset \mathbb{R}^N$ is a bounded domain, then the **signed distance function** to the boundary $\partial\Omega$ is the function $\mathbb{R}^N \ni x \mapsto d_\Omega(x)$ defined by :

$$d_\Omega(x) = \begin{cases} -d(x,\partial\Omega) & \text{if } x \in \Omega \\ 0 & \text{if } x \in \partial\Omega \\ d(x,\partial\Omega) & \text{if } x \in \left(\mathbb{R}^N \setminus \overline{\Omega}\right) \end{cases},$$

where $d(x,\partial\Omega)$ is the usual Euclidean distance from x to $\partial\Omega$.
Very often, the Hamilton-Jacobi equation (5) is initialized, or re-initialized, with the signed distance function. However, at later times t, the level set function $\psi(t,x)$, solution of (5), is not a signed distance function. Furthermore, the functions ψ and d_Ω do not share the same boundary conditions (see [9] for details). Therefore one cannot retrieve geometrical informations on the shape $\Omega(t)$ from $\psi(t,x)$. However, at every time t it is not hard to compute the signed distance function of $\Omega(t)$. As in the case of thickness constraints [9], we shall use this signed distance function to get all necessary information for the formulation of our molding constraints.

3.3 Ersatz material

Using the so-called "ersatz material" approach, we extend the state equations to the whole domain D. To do this, we fill the holes $D \setminus \Omega$ by a weak phase that mimics the void, but at the same time avoids the singularity of the rigidity matrix. More precisely, we define an elasticity tensor $A^*(x)$ which is a mixture of A in Ω and of the weak material mimicking holes in $D \setminus \Omega$

$$A^*(x) = \rho(x)A \quad \text{with} \quad \rho = \begin{cases} 1 & \text{in } \Omega, \\ 10^{-3} & \text{in } D \setminus \Omega. \end{cases} \tag{6}$$

Decomposing the boundary ∂D of the working domain in three parts

$$\partial D = \partial D_D \cup \partial D_N \cup \partial D_0,$$

and demanding that the shape boundary $\partial\Omega = \Gamma_D \cup \Gamma_N \cup \Gamma_0$ must further satisfy

$$\Gamma_D \subset \partial D_D, \quad \Gamma_N \subset \partial D_N,$$

where ∂D_0 supports homogeneous Neumann boundary conditions, the displacement u is finally computed as the solution of

$$\begin{cases} -\mathrm{div}\,(A^* e(u)) = f & \text{in } D, \\ u = 0 & \text{on } \partial D_D, \\ \big(A^* e(u)\big)n = g & \text{on } \partial D_N, \\ \big(A^* e(u)\big)n = 0 & \text{on } \partial D_0. \end{cases} \tag{7}$$

4 Casting process

We give in this section a short description of the casting process. A simplified sequence of steps for the construction of a cast part is the following:

1. Molds are used in order to create a cavity, having the shape of the structure that we intend to construct.
2. The cavity is filled with molten liquid metal.
3. The liquid solidifies.
4. The molds are removed and the cast part is revealed.

There are many different types of casting (metal casting, sand casting, investment casting, etc.) and the choice among them depends on the type of cast part. Each type inserts different constraints on the casting process. We address the interested reader to [19] for a complete presentation of the casting process. Here we confine ourselves to **permanent mold casting**, in which the molds are removed without being destroyed. We call **parting direction** the direction along which one mold is removed and **parting surface**, the surface on which different molds come in contact [46]. Note that several molds can be used in the casting system and each one has its own parting direction (see Figure 3). The parting surface between two molds can be predefined or it can be constructed after the optimization using suitable methods [1, 22]. In most of the industrial applications, planar parting surface are preferred because of reasons of cost and simplicity [46].

Each of the above steps introduces different constraints in the shape of the cast part. In this work we are mainly interested to ensure the feasibility of the last step, i.e. the removal of the molds. Thus, we need to impose that the cast part has such a shape, so that the molds can actually be removed after the end of the solidification process. Let us give a 2d example of the above mentioned. Suppose that for an optimization problem like the one described by equations (1) to (4) we obtain the optimized shape Ω, shown in Figure 2. In Figure 3 we see that depending on the molding system considered, this shape can be moldable or not. In the right figure of Figure 3, some parts of the shape oppose to the removal of the molds in their corresponding parting direction.

The construction of the casting system is usually based on the intuition of the caster. Changes on the number and on the position of the molds can turn a non-moldable shape to a moldable one. The design of the whole casting system is very difficult (if possible) to be formulated mathematically and be subjected to optimization. Works in this direction are mostly concerned with parametric or shape optimization of parts of the molds [30, 43] or of the riser [42]. In the present paper, we do not consider the

optimization of the casting process, but the molding system is considered a priori defined.

5 Formulation of the molding direction constraint

5.1 Molding direction condition on design velocity

A molding direction condition on the design velocity was proposed by Xia et al. in [46], which is inspired by Fu et al. [22]. According to these authors, if a shape is feasible with respect to the molding direction specification for its corresponding molding system, then the boundary of the structure $\partial\Omega$ can be divided into m disjoint parts Γ_i, $i = \{1,...,m\}$, such that $\Gamma_i \cap \Gamma_j = \emptyset$, $j = \{1,...,m\}$, $\overline{\cup_{i=1}^{m} \Gamma_i} = \partial\Omega$ and Γ_i can be parted in the direction d_i. Thus, a molding direction condition for this shape is

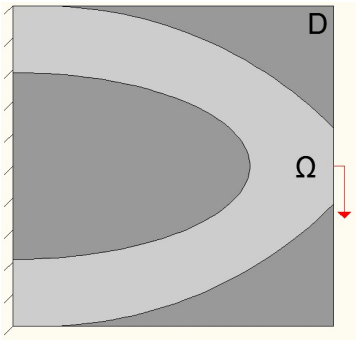

Fig. 2 Possible optimized shape of a cast part.

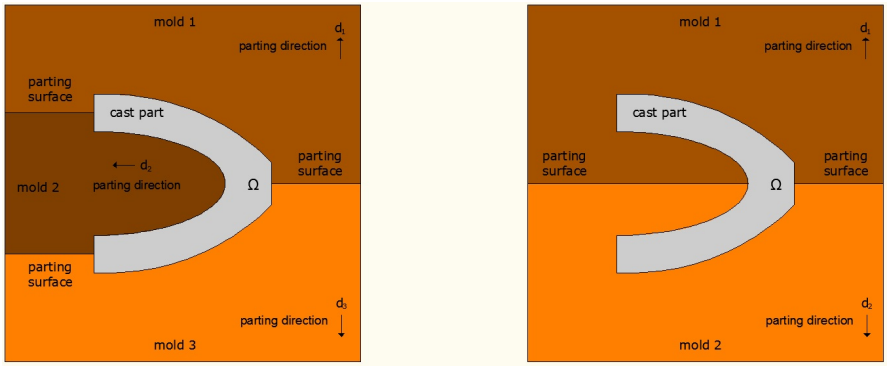

Fig. 3 Left: moldable shape; right: non-moldable shape.

$$d_i \cdot n(x) \geq 0, \quad \forall x \in \Gamma_i, \tag{8}$$

where $n(x)$ is the exterior unit normal at $x \in \Gamma_i$. The shape on the left in Figure 4 satisfies the condition (8), while the shape on the right does not. In fact, as it is mentioned in [46], undercuts (slots that hint the removal on the mold in its parting direction) and interior voids are not allowed.

Based on the the molding condition (8), Xia et al. [46] proposed the following method : starting from a shape **that satisfies the constraint (8)**, consider an advection velocity of the form

$$\theta_i(x) = \lambda(x) d_i, \quad \forall x \in \Gamma_i. \tag{9}$$

In this way, the shape remains always moldable, since no undercut can be created during the advection of the shape with this type of velocity and no interior void can be nucleated. The topological changes that can occur using this advection velocity cannot turn the shape from moldable to non-moldable [46].

This method, despite its simplicity and effectiveness, presents two major drawbacks. First, the shape must be initialized as being castable so that it can satisfy the mold-

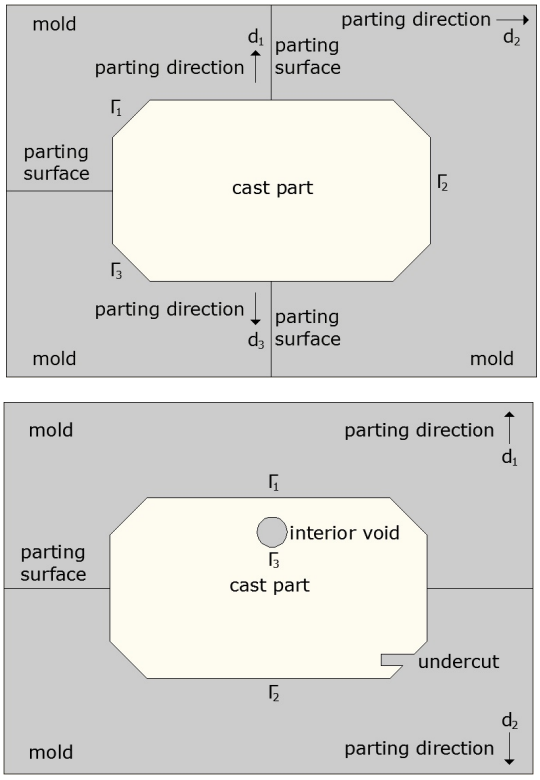

Fig. 4 Top: moldable shape; bottom: non-moldable shape.

ing constraint during the entire optimization process ; this is a severe limitation on the choice of admissible initial guess shapes. Nevertheless, if such an initialization can be found, then it turns out that the method is flexible enough, especially in 3d, in order for complicated topologies to appear from very trivial initializations. Second, and more important from our point of view, the very form (9) of the advection velocity does not allow all possible deformations of the shape, including those which are required for some other constraints. As it is stated in [46], there is no component of the advection velocity normal to the parting direction. Therefore, the shape can shrink by extinction of some part, but it cannot expand normal to its corresponding parting direction. As an example, consider the case where a minimum thickness constraint is also applied [9]. Then, if the measured thickness is in a direction orthogonal to the parting direction, the shape cannot expand in this orthogonal direction (in order to meet the constraint of minimal thickness) because it can move only parallel to its parting direction. Therefore, in such a situation, the thickness constraint will not be respected. Therefore, it is necessary to formulate a more general molding constraint, free of the above limitations.

5.2 Generalised molding constraint

A first idea for a generalized way to treat the molding direction constraint consists simply in regarding (8) as a pointwise constraint in our optimization problem. Then, it can be exactly penalized as we shall do in (16) to compute its shape derivative.
A second idea is to use the signed distance function to the boundary of the domain to derive all necessary information, as we have done for thickness constraints in [9]. Denoting Ω the actual shape and D the design domain, a generalized molding direction constraint can be formulated as:

$$d_\Omega\left(x+\xi d_i\right) \geq 0 \quad \forall x \in \Gamma_i, \forall \xi \in [0, dist(x, \partial D)]\,, \tag{10}$$

or equivalently

$$d_\Omega\left(x+\xi d_i\right) \geq 0 \quad \forall x \in \Gamma_i, \forall \xi \in [0, diam(D)]\,, \tag{11}$$

where we denote $diam(D) = sup_{x,y}\left\{dist(x,y), x, y \in D\right\}$ the diameter of the fixed domain D. We prefer to use formulation (11) instead of (10), in order to avoid the dependence of the term $dist(x, \partial D)$ on the shape Ω.
Intuitively, this formulation says that, starting from a point on the boundary, which will be casted in the direction d_i and travelling along this direction, we should not meet again some part of the structure (see Figure 5). In case that the parting surface is not defined a priori, but is revealed at a second step after the design has been completed and for a system of two molds (see Figure 3, right image), the constraint (11) becomes:

$$d_\Omega\left(x+\xi sign(n\cdot d)d\right) \geq 0 \quad \forall x \in \partial\Omega, \forall \xi \in [0, diam(D)]\,. \tag{12}$$

5.3 Uniform cross-section surface constraint

Another useful constraint for cast parts is the so-called "uniform cross-section surface constraint" [48], since it simplifies a lot the shape of the desired molds. To our knowledge, Yamada et al. [48] were the first to study this type of constraint in shape and topology optimization using a combination of a phase-field and a level-set method. The constraint states that the cast part should have a uniform constant thickness along some direction d. An example of a uniform cross-section cantilever of thickness h is given in Figure 6. The boundary conditions may not be uniform along this direction and therefore the problem cannot be reduced to a 2d problem. We can formulate this type of constraint at least in two ways. The first formulation states that the normal to the boundary cannot have a non-zero component in this direction d:

$$d \cdot n(x) = 0, \quad \forall x \in \partial\Omega \setminus \partial D. \tag{13}$$

A second way to enforce the constraint is to limit the admissible advection fields θ. Starting from an initial guess shape that has a uniform cross-section along the desired direction d and constraining the advection fields to be zero along this direction, the thickness along d will not change. In fact, this is the easiest way to follow, since no mathematical constraint is imposed in the optimization process and the calculation of the velocity field is reduced to a 2d problem, as we will see in the next section.

By enforcing the constraint (13), the feasibility of the shape is guaranteed for casting along the direction d, i.e. this constraint is a sufficient but not a necessary condition.

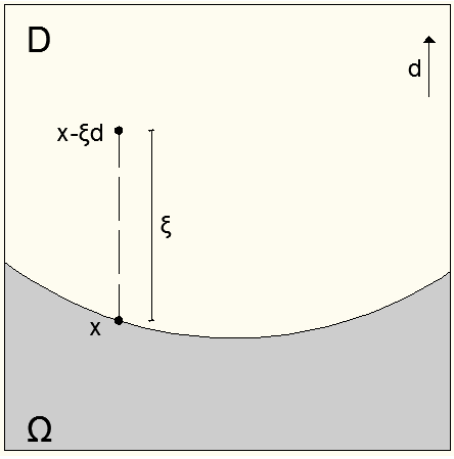

Fig. 5 Checking castability along the parting direction d at the point $x \in \partial\Omega$.

6 Shape derivative

6.1 Derivative of the condition on design velocity

Xia et al. proposed in [46] a modification of the advection velocity according to (9), that guarantees a descent direction. Starting from the general form of the shape derivative for a functional $J(\Omega)$

$$J'(\Omega)(\theta) = \int_{\partial\Omega} \theta(s)\cdot n(s) V(s) ds = \sum_{i=1}^{m} \int_{\Gamma_i} \theta_i(s)\cdot n(s) V_i(s) ds$$

and considering admissible advection fields of the type (9), we get

$$J'(\Omega)(\theta) = \sum_{i=1}^{m} \int_{\Gamma_i} \lambda_i(s) d_i \cdot n(s) V_i(s) ds,$$

and choosing

$$\lambda_i(s) = -V_i(s) d_i \cdot n(s), \forall i = 1, ..., m$$

for each part Γ_i of the boundary $\partial\Omega$, the shape derivative becomes

$$J'(\Omega)(\theta) = -\sum_{i=1}^{m} \int_{\Gamma_i} (d_i \cdot n(s))^2 (V_i(s))^2 ds \leq 0,$$

which shows that the chosen advection velocity

$$\theta_i(s) = -V_i(s)(d_i \cdot n(s)) d_i, \forall i = 1, ..., m \tag{14}$$

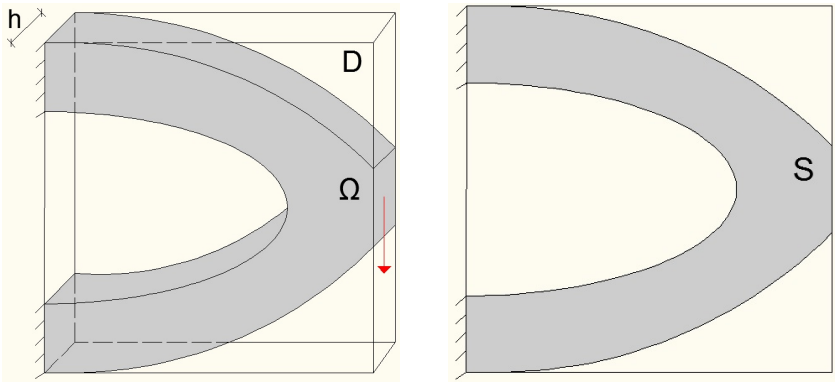

(a) (b)

Fig. 6 (a): uniform cross-section cantilever of thickness h; (b): cross-section S.

is indeed a descent direction. We replace the Hamilton-Jacobi equation (5) by the linear transport equation

$$\frac{\partial \psi}{\partial t} + \theta \cdot \nabla \psi = 0, \tag{15}$$

where the vectorial velocity θ is an extension of the advection velocity (14) and the normal n is the normal associated with the initial shape.

6.2 Derivative of the generalized molding constraint

We start with the derivation of constraint (8). One advantage of this constraint is that it is of local nature, i.e. it contains information only for points on the boundary without searching along rays emerging from them. On the other hand, it contains the exterior normal vector, whose derivation is more complicated than the one of the signed distance function. In a first step, a global penalty functional can be formulated as

$$P_{GMC}(\Omega) = \int_{\partial\Omega} [(d \cdot n(s))^-]^2 ds, \tag{16}$$

with the usual notations $(f)^+ = \max(f,0)$ and $(f)^- = \min(f,0)$.

Proposition 1. *For a smooth shape Ω, the shape derivative of (16) reads*

$$P'_{GMC}(\Omega)(\theta) = \int_{\partial\Omega} \theta(s) \cdot n(s) \Big(2d \cdot \nabla_s (d \cdot n(s))^- - H(s)[(d \cdot n(s))^-]^2 \Big) ds, \tag{17}$$

where H is the mean curvature and ∇_s the tangential gradient.

Proof. Using a classical result about shape derivation of integrals with shape-dependent integrands (see Proposition 6.28 in [2]), the shape derivative of (16) reads

$$\begin{aligned}
&P'_{GMC}(\Omega)(\theta) = \\
&\int_{\partial\Omega} \theta(s) \cdot n(s) \big[H(s)[(d \cdot n(s))^-]^2 + \frac{\partial([(d \cdot n(s))^-]^2)}{\partial n} \big] ds \\
&+ \int_{\partial\Omega} \frac{\partial([(d \cdot n(s))^-]^2)}{\partial \Omega}(\theta) ds = \\
&\int_{\partial\Omega} \theta(s) \cdot n(s) \big[H(s)[(d \cdot n(s))^-]^2 + 2(d \cdot n(s))^- \frac{\partial (d \cdot n(s))}{\partial n} \big] ds \\
&+ \int_{\partial\Omega} 2(d \cdot n(s))^- d \cdot n'(s)(\theta) ds = \\
&\int_{\partial\Omega} \theta(s) \cdot n(s) \big[H(s)[(d \cdot n(s))^-]^2 + 2(d \cdot n(s))^- d \cdot ((\nabla n) n) \big] ds \\
&+ \int_{\partial\Omega} 2(d \cdot n(s))^- d \cdot n'(s)(\theta) ds,
\end{aligned} \tag{18}$$

where $n'(s)(\theta)$ is the shape derivative of the normal. Under the smoothness assumption on the shape, there exists an extension of the unit normal in a tubular area around the boundary by $n(x) = \nabla d_\Omega(x)$. Now, the unit normal satisfies the equa-

tion $|n(x)|^2 = 1$ from which differentiating both sides, we obtain $(\nabla n)n = 0$. Thus, equation (18) reduces to

$$\begin{aligned} P'_{GMC}(\Omega)(\theta) = &\int_{\partial\Omega} \theta(s)\cdot n(s) H(s)[(d\cdot n(s))^-]^2 ds \\ &+ \int_{\partial\Omega} 2(d\cdot n(s))^- d\cdot n'(s)(\theta) ds. \end{aligned} \tag{19}$$

What remains is the calculation of the shape derivative of the unit normal to the boundary. From Lemma 4.8 in [34], we have that the transported of the unit normal $n(\Omega,x)$ is

$$\begin{aligned} n((Id+\theta)(\Omega), x+\theta(x)) &= \frac{((I+\nabla\theta)^{-1})^T n}{|((I+\nabla\theta)^{-1})^T n|} \\ &= \frac{n-(\nabla\theta)^T n + o(\theta)}{1-(\nabla\theta)^T n\cdot n + o(\theta)} \\ &= (n-(\nabla\theta)^T n + o(\theta))(1+(\nabla\theta)^T n\cdot n + o(\theta)) \\ &= n(\Omega,x) - (\nabla\theta)^T n + ((\nabla\theta)^T n\cdot n)n + o(\theta), \end{aligned}$$

and so the Lagrangian shape derivative of the unit normal is

$$Y(\theta,x) = -(\nabla\theta)^T n + ((\nabla\theta)^T n\cdot n)n.$$

Since by the Hadamard structure theorem [2], [27], [34], [39], the shape derivative in the direction θ depends only on the normal component $\theta\cdot n$ on the boundary $\partial\Omega$, we can restrict our attention to a vector field $\theta(x)$ of the form $\theta(x) = w(x)n(x)$, where w is any scalar function. In such a case, we find that $(\nabla n)^T\theta = w(x)(\nabla n)^T n = 0$ and thus

$$\begin{aligned} Y(\theta,x) &= -(\nabla\theta)^T n - (\nabla n)^T\theta + ((\nabla\theta)^T n\cdot n)n + ((\nabla n)^T\theta\cdot n)n \\ &= -\nabla(\theta\cdot n) + \big[n\cdot\nabla(\theta\cdot n)\big]n \\ &= -\nabla_s(\theta\cdot n) \\ &= -\nabla_s(w(x)). \end{aligned}$$

The Eulerian shape derivative of the unit normal reads

$$n'(x)(\theta) = Y(\theta,x) - \nabla n\theta(x) = Y(\theta,x) = -\nabla_s(w(x)).$$

The same result was found in [28], using similar variational principles. In view of the above results, equation (19) becomes

$$P'_{GMC}(\Omega)(\theta) = \int_{\partial\Omega} w(s)H(s)[(d\cdot n(s))^-]^2 ds - \int_{\partial\Omega} 2(d\cdot n(s))^- d\cdot\nabla_s w(s) ds.$$

On the other hand, using the identity (see [28])

$$\int_{\partial\Omega} a\cdot\nabla_s b\, ds + \int_{\partial\Omega} (\nabla_s\cdot a) b\, ds = \int_{\partial\Omega} a\cdot n H\, b\, ds,$$

where a is a vector field and b is a scalar field, we deduce

$$P'_{GMC}(\Omega)(\theta) = \int_{\partial\Omega} w(s)\big(\nabla_s \cdot (2(d\cdot n(s))^- d) - H(s)[(d\cdot n(s))^-]^2\big)ds$$
$$= \int_{\partial\Omega} w(s)\big(2d\cdot\nabla_s(d\cdot n(s))^- - H(s)[(d\cdot n(s))^-]^2\big)ds,$$

which completes the proof.

Lemma 1. *The shape derivative (17) can be also written in the form*

$$P'_{GMC}(\Omega)(\theta) =$$
$$\int_{\partial\Omega} \theta(s)\cdot n(s)\left(\sum_{i=1}^{N-1} \kappa_i(s)(d\cdot e_i(s))^2(-sign((d\cdot n(s))^-)) - H(s)[(d\cdot n(s))^-]^2\right)ds,$$

where κ_i are the principal curvatures of $\partial\Omega$ at a point $s\in\partial\Omega$ and e_i the associated principal curvature directions ($i=1,...,N-1$).

Proof. For a point $s\in\partial\Omega$ we can write $\nabla_s n(s)$ in the form (see [4]):

$$\nabla_s n(s) = \sum_{i=1}^{N-1} \kappa_i(s) e_i(s)\otimes e_i(s). \tag{20}$$

Substituting (20) in (17) yields the desired result.

We now switch to the derivation of the other constraints (11) and (12), which are pointwise constraints of the same type as the minimum thickness constraint in [9]. Therefore, the same steps need to be followed for their shape derivation and the final extraction of a descent direction. For the sake of completeness, let us mention once more the basic steps of this procedure.

For constraint (11) we formulate a penalty functional of the form

$$P_{GMC}(\Omega) = \sum_{i=1}^{m}\int_{\Gamma_i}\int_0^{diam(D)} \left[(d_\Omega(s+\xi d_i))^-\right]^2 d\xi ds,$$

while for constraint (12), it reads

$$P_{GMC}(\Omega) = \int_{\partial\Omega}\int_0^{diam(D)} \left[(d_\Omega(s+\xi\, sign(n(s)\cdot d)d))^-\right]^2 d\xi ds.$$

The two functionals are of the same type and can be written in compact notation (see Figure 7)

$$P_{GMC}(\Omega) = \int_{\partial\Omega}\int_0^{diam(D)} \left[(d_\Omega(x_m))^-\right]^2 d\xi dx, \tag{21}$$

where x_m denotes an offset point of the boundary which is either $x_m = x+\xi d_i$ or $x_m = x+\xi\, sign(n(x)\cdot d)d$.
The following result was obtained in [9] and we recall it without proof.

Proposition 2. *The shape derivative of (21) reads*

$$P'_{GMC}(\Omega)(\theta) = \int_{\partial\Omega}\int_0^{diam(D)} \theta(x)\cdot n(x)\left[H\left((d_\Omega(x_m))^-\right)^2 + 2\left((d_\Omega(x_m))^-\right)\nabla d_\Omega(x_m)\cdot\nabla d_\Omega(x)\right] d\xi dx - \int_{\partial\Omega}\int_0^{diam(D)} \theta\left(x_{m|\Omega}\right)\cdot n\left(x_{m|\Omega}\right) 2\left(d_\Omega(x_m)\right)^- d\xi dx,$$

where $x_{m|\Omega}$ is the orthogonal projection of x_m on $\partial\Omega$.

The advantage of the formula of Proposition 2, compared to that of Proposition 1, is that it does not contain any tangential derivative of the normal, or equivalently principal curvatures, which are notably hard to compute with great accuracy.

Remark 1. As already noticed in [9], a descent direction can be found in a second step, after identifying the linear form of the shape derivative with another scalar product. The idea is similar to that of regularization, as described in [20]. More precisely, solving the variational formulation

$$\int_D \left(\alpha_{reg}^2 \nabla Q\cdot\nabla v + Qv\right) dx = P'(\Omega)(v) \quad \forall v \in H^1(D), \tag{22}$$

where $\alpha_{reg} > 0$ is a positive number (of the order of the mesh size) which controls the regularization width, yields a solution $Q \in H^1(D)$. Then, choosing a vector field $\theta = -Qn$, we obtain a guaranteed descent direction for P_{GMC} since, taking $v = -Q$ in (22), we get

$$P'_{GMC}(\Omega)(-Qn) = -\int_D \left(\alpha_{reg}^2 |\nabla Q|^2 + Q^2\right) dx.$$

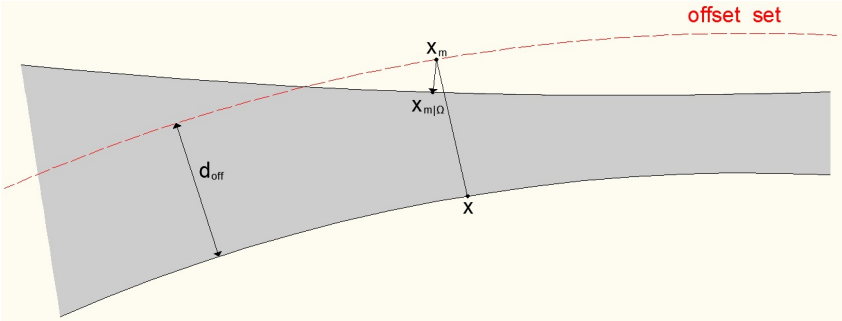

Fig. 7 Offset point x_m and its projection $x_{m|\Omega}$ on the boundary.

6.3 Derivative of the uniform cross-section constraint

For the constraint (13), a quadratic penalty functional reads

$$P_{UCS}(\Omega) = \int_{\partial\Omega\setminus\partial D} (d\cdot n(s))^2 ds, \tag{23}$$

which highly ressembles (16) and thus its shape derivation is omitted here.

If we work in the feasible set of shapes which are constant in the direction d, it is even simpler to take into account this constraint. We consider shapes $\Omega = S\times[0,h]$ where S is a surface perpendicular to d (see Figure 6). In this case, we force the advection velocity to be zero along the direction d of uniform thickness. Starting from the general formula of a shape derivative

$$J'(\Omega)(\theta) = \int_{\partial\Omega} V(s)\theta(s)\cdot n(s) ds,$$

where $\partial\Omega = \partial S\times[0,h]$, we use Fubini's theorem for the shape derivative

$$J'(\Omega)(\theta) = \int_{\partial S}\int_0^h V(\xi)\theta(s)\cdot n(s) d\xi ds = \int_{\partial S}\theta(s)\cdot n(s)\int_0^h V(\xi) d\xi ds.$$

From this, a descent direction is revealed for the uniform cross-section optimizable boundary ∂S with the choice

$$\begin{cases} \theta(s) = -n(s)\displaystyle\int_0^h V(\xi)d\xi, \quad \forall s \text{ on } \partial S, \\ \theta(s)\cdot d = 0, \quad \forall s \text{ on } \partial S, \end{cases} \tag{24}$$

where $n(s)$ is the normal to ∂S which satisfies $n\cdot d = 0$. Another, simple way to treat this constraint is through the regularization of the velocity field via equation (22). Choosing α_{reg} to be a tensor, instead of a positive scalar, we can smooth the advection field in an anisotropic way. Then, equation (22) is rewritten as

$$\int_D \left(\sum_{i=1}^N a_i^2 \frac{\partial Q}{\partial x_i}\frac{\partial v}{\partial x_i} + Qv \right) dx = J'(\Omega)(v) \quad \forall v\in H^1(D), \tag{25}$$

where $\alpha_{reg} = \sum_{i=1}^N a_i e_i\otimes e_i$ is the regularization tensor in the canonical basis $(e_i)_{i=1,\dots,N}$ of $\mathbb{R}^N$. For example, if we want a vector field θ of the type of (24) with $d = e_2$, we can set $a_2 >> a_i, i\neq 2$. Then, the solution Q of (25) will be constant in the x_2 direction and the descent direction $\theta = -Qn(s)$, where $n(s)$ is the normal to ∂S, satisfies $\theta\cdot d = 0$. In other words, starting from an initial shape that respects the constraint and regularizing the advection field in the way just described, we obtain a final optimized shape with a uniform cross-section.

7 Numerical examples

We have coded all numerical examples herein in the finite element software SYSTUS of ESI-Group [40]. A quadrangular mesh has been used both for the solution of the elasticity system and for the level set function. For the elasticity analysis, Q1 finite elements have been used, the Young modulus E is normalized to 1 and the Poisson ratio ν is set to 0.3. The "ersatz material" is considered to have the same Poisson ratio, while its Young modulus is set to 10^{-3}.

7.1 Molding direction

The three-dimensional box-like structure of Figure 8 is our test case to apply several molding direction constraints and compare the corresponding optimized shapes. The entire domain is used for the analysis and is discretized using $40 \times 40 \times 20$ $Q1$ elements. We minimize the compliance under an equality constraint for the volume. The optimization problem reads

$$\begin{aligned} &\min_{\Omega \in \mathscr{U}_{ad}} \int_{\partial\Omega} g \cdot u ds \\ &\text{s.t.} \int_{\Omega} dx = a_V |D|, \end{aligned} \tag{26}$$

where u is the solution of (7) and $a_V \in [0,1]$ determines the final volume of the structure as percentage of the volume of the working domain D. An augmented Lagrangian method is used here to enforce the constraints, as in our previous work [9]. We refer to [11] for the formula of the shape derivative for the compliance.
At a first step, we impose no molding constraint and solve the optimization problem (26) for $a_V = 0.2$ using the arbitrary initialization of Figure 9(a). The optimized shape after 250 iterations is shown in Figure 9(b).

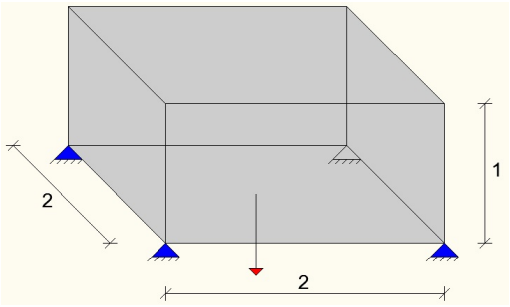

Fig. 8 Boundary and loading conditions for a 3d box.

Let us now solve the same optimization problem for a cast part that must comply with a predefined molding system. For example, if we want to use one mold in the design domain D, remove it in the direction $d = (0,0,1)$ and impose the plane $z = 0$ to be a possible parting surface, then obviously the shape in Figure 9(b) is no more feasible. Of course, we cannot hope that starting with a different, even much simpler, initialization, we can obtain a castable optimized shape without enforcing a molding direction constraint.
As we have mentioned before, in the absence of thickness constraints, we believe that the method of [46], as described in section 5.1, gives quite satisfying results with a very simple implementation. The only restriction is that the initial design must satisfy the constraint. For later iterations it is enough to impose the molding direction condition on the design velocity. Starting with a full-domain initialization (see Figure 10(a)) and taking the initial level-set function equal to the signed distance function to the upper part of the domain, we choose an advection velocity of the type (9), where $d = (0,0,1)$, and we obtain the optimized shape of Figure 10(b). A comparison of the performance with the previous test case is proposed on Figure 11.

More flexibility in shape variations is given if the casting direction is set as $d = (0,0,1)$ and no parting surface is imposed. In this case, the design domain D can contain two molds, one removed in the direction d and the second in the opposite direction $(-d)$. The same full-domain initialization, with the signed distance function to the upper part of the domain, could be chosen, but this would unfortunately

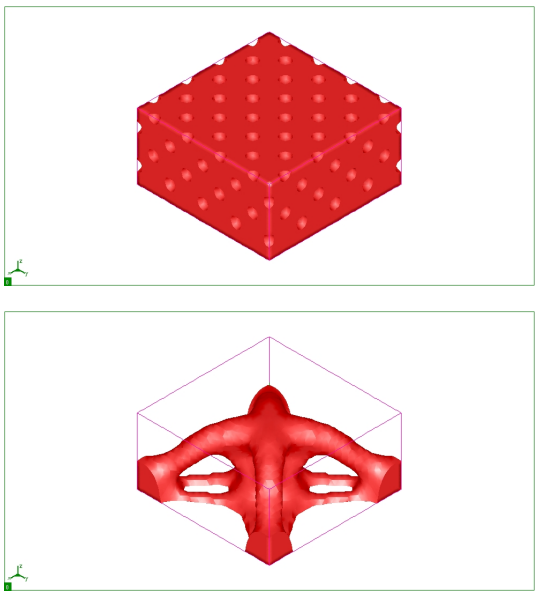

Fig. 9 Initialization (top) and optimized shape (bottom) for the optimization problem (26) without a molding constraint.

result in a final system with just one mold. Instead, it is more efficient to take the initial level-set function equal to the signed distance function both to the upper and lower part of the domain. The optimized shape is shown in Figure 12(b).

As expected, a completely different optimized shape is obtained if we change the casting direction. Separating the molds horizontally, in the direction $d = (1,0,0)$ and imposing no specific parting surface, yields the optimized shape of Figure 14. In both Figures 12 and 14 we see that topological changes can take place by "pinching a thin wall" [11], even though we started from a full-domain initialization.

Molding direction & Maximum Thickness

A constraint on the maximum local thickness can be combined with the molding condition on the design velocity without any difficulty a priori. The reason is that the maximum thickness constraint gradient will be of uniform sign, tending always to reduce the thickness (and the volume) of the shape. As we have mentioned in section 5.1, when an advection velocity of the type (9) is chosen, the shape can shrink, but not expand normal to the casting direction. Adding a maximum thickness constraint to the test case of Figure 10, where the shape is casted along the direction $d = (0,0,1)$ and the plane $z = 0$ is chosen as a possible parting surface, we solve the optimization problem

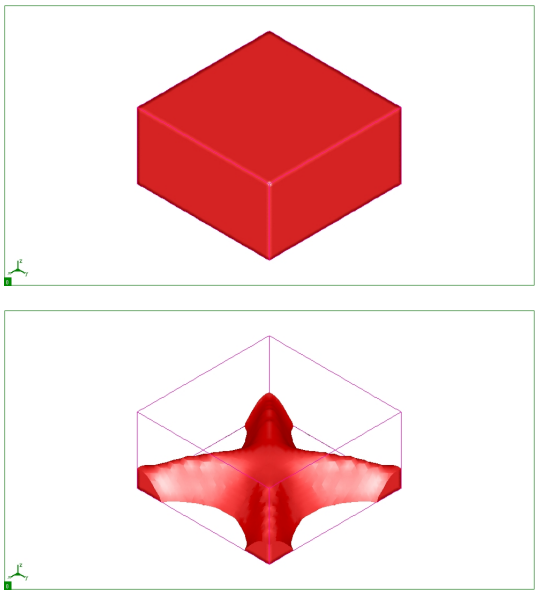

Fig. 10 Initialization (top) and optimized shape (bottom) for the optimization problem (26), setting $d = (0,0,1)$ as casting direction, $z = 0$ as a possible parting surface and using the molding direction condition (9).

$$\begin{aligned} &\min_{\Omega\in\mathscr{U}_{ad}} \int_{\partial\Omega} g\cdot u ds \\ &\text{s.t.} \int_{\Omega} dx = a_V|D|, \\ &\qquad P_{MaxT}(\Omega) = \left(\frac{\int_{\Omega} f(d_\Omega(x))d_\Omega(x)^2 dx}{\int_{\Omega} f(d_\Omega(x))dx}\right)^{\frac{1}{2}} \leq d_{max}/2, \end{aligned} \tag{27}$$

where $d_{max} = 0.2$ and f is a regularization function that reads (see [9]):

$$f(d_\Omega(x)) = 0.5\left(1+\tanh\left(\frac{|d_\Omega(x)|-d_{max}/2}{\alpha_f d_{max}/2}\right)\right),$$

$\alpha_f > 0$ being a parameter that controls the regularization of the constraint. Using the same initialization as in Figure 10(a) and enforcing $z = 0$ as the only possible parting surface, the optimized shape after 250 iterations and the convergence diagrams are shown in Figures 16 and 17.

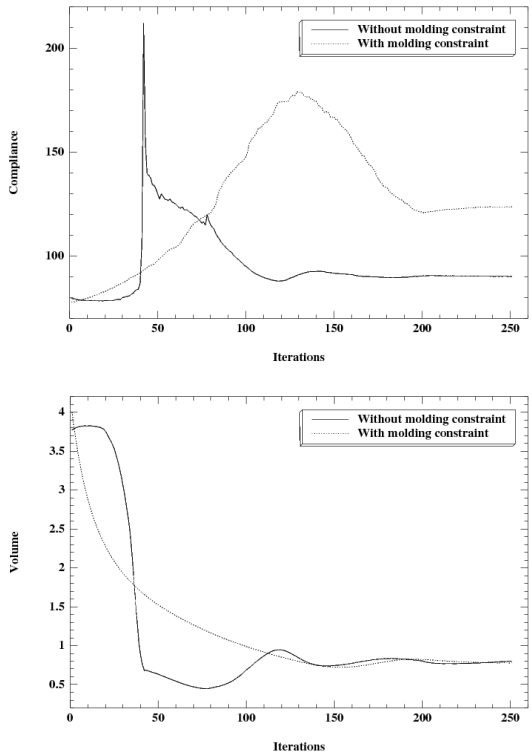

Fig. 11 Compliance (top) and volume (bottom) convergence histories for the results in Figures 9(bottom) and 10(bottom).

Molding direction & Minimum Thickness

Suppose now that we want to add a minimum thickness constraint with $d_{min} = 0.4$ in the shape of Figure 10(b). The molding condition (9) is no more a suitable method to follow (see section 5.1) and we shall instead combine a minimum thickness constraint with the generalized molding constraint (10). The previously optimized shape is taken as an initial guess to solve the problem

$$\begin{aligned} &\min_{\Omega\in\mathscr{U}_{ad}} \int_{\partial\Omega} g\cdot u ds \\ &\text{s.t.} \int_{\Omega} dx = a_V|D|, \\ &\quad P_1(\Omega) = P_{MinT}(\Omega) = \int_{\partial\Omega}\int_0^{d_{min}} \left[\left(d_\Omega\left(s-\xi n(s)\right)\right)^+\right]^2 d\xi ds = 0, \\ &\quad P_2(\Omega) = P_{GMC}(\Omega) = \int_{\partial\Omega}\int_0^{diam(D)} \left[\left(d_\Omega\left(s+\xi d\right)\right)^-\right]^2 d\xi ds = 0, \end{aligned} \tag{28}$$

without any condition on the advection velocity. An optimized shape for the optimization problem (28) is shown in Figure 18(b). The convergence diagrams for the penalty functionals P_1 and P_2 are shown in Fig.19.

We now switch to a minimum thickness constraint of $d_{min} = 0.3$ and to the case of two mold in the z-direction, as applied to the shape of Figure 12(b). In this case, the optimization problem reads

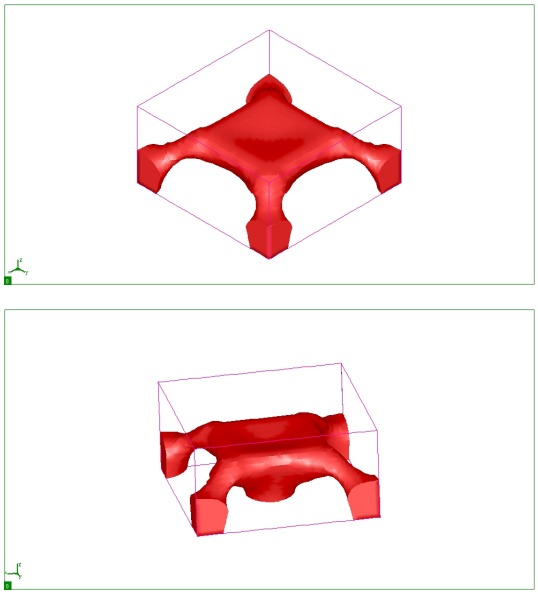

Fig. 12 Plots of the optimized shape for the optimization problem (26), setting $d = (0,0,1)$ as casting direction, no a priori defined parting surface and using the molding direction condition (9).

$$\begin{aligned}
&\min_{\Omega\in\mathscr{U}_{ad}} \int_{\partial\Omega} g\cdot uds \\
&\text{s.t.} \int_{\Omega} dx = a_V|D|, \\
&\qquad P_1(\Omega) = P_{MinT}(\Omega) = \int_{\partial\Omega}\int_0^{d_{min}} \left[\left(d_\Omega\left(s-\xi n(s)\right)\right)^+\right]^2 d\xi ds = 0, \\
&\qquad P_2(\Omega) = P_{GMC}(\Omega) = \int_{\partial\Omega}\int_0^{diam(D)} \left[\left(d_\Omega\left(s+\xi sign(n\cdot d)d\right)\right)^-\right]^2 d\xi ds = 0
\end{aligned} \tag{29}$$

Note that the constraint $P_2(\Omega)$ is different from that in (28). We obtain the optimized shape of Figure 20. The convergence diagrams for the penalty functionals P_1 and P_2 are shown in Figure 21.

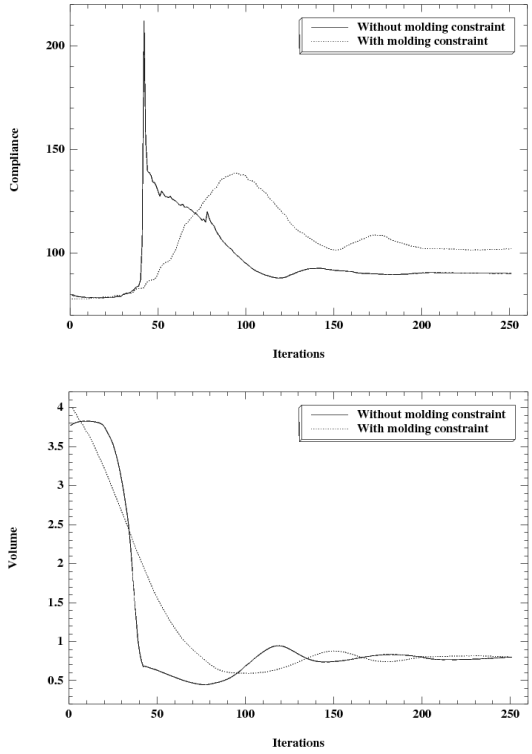

Fig. 13 Compliance (top) and volume (bottom) convergence diagrams for the results in Figures 9(bottom) and 12.

Table 1 Compliance of the optimized structures.

	Compliance
Without molding constraint (Figure 9(bottom)).	90.14
With casting direction $d = (0,0,1)$ and no parting surface (Figure 12).	102.07
With casting direction $d = (0,0,1)$, no parting surface and minimum thickness constraint (Figure 20(bottom)).	105.87
With casting direction $d = (1,0,0)$ and no parting surface (Figure 14).	114.13
With casting direction $d = (0,0,1)$ and parting surface at $z = 0$ (Figure 10(bottom)).	123.68
With casting direction $d = (0,0,1)$, parting surface at $z = 0$ and minimum thickness constraint (Figure 18(bottom)).	134.68
With casting direction $d = (0,0,1)$, parting surface at $z = 0$ and maximum thickness constraint (Figure 16).	143.65

7.2 Uniform cross-section

The $2 \times 0.5 \times 1$ three dimensional cantilever of Figure 22, discretized by $40 \times 10 \times 20$ $Q1$ elements, is chosen as test case to apply the uniform cross-section surface

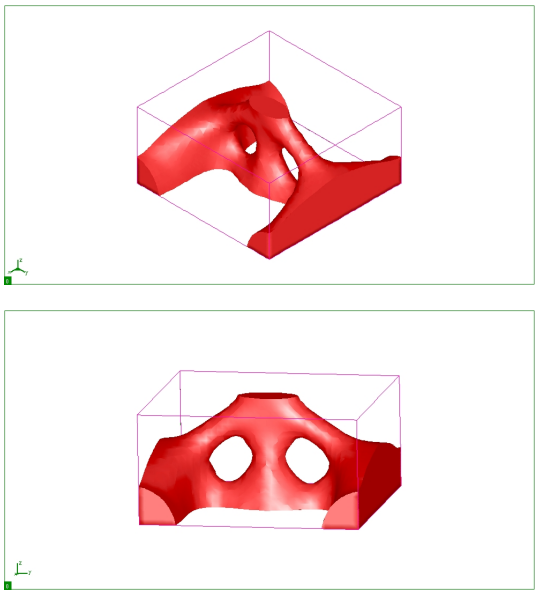

Fig. 14 Plots of the optimized shape for the optimization problem (26), setting $d = (1,0,0)$ as casting direction, no a priori defined parting surface and using the molding direction condition (9).

constraint. It is clamped on one side and, at the middle of its opposite side, a unitary vertical load is applied. At a first step, problem (26) is solved for $a_V = 0.25$ without imposing any further geometric constraint on the shape. Starting from the arbitrarily perforated shape of Figure 23(a), we obtain after 200 iterations the optimized shape of Figure 23(b).

We now look for an optimized shape with a uniform cross-section along the y-axis. Starting from the initial shape of Figure 24(a), which has five uniform holes along this direction, we regularize at each iteration the velocity field for the advection of the shape in an anisotropic way, based on equation (25), with a much higher regularization coefficient in the y-direction ($a_y >> a_x, a_z$). In our example, $a_x = a_z = 2\Delta x$, Δx being the uniform mesh size, has been used to regularize the advection velocity in a small region around the shape boundary in the direction of the x- and z-axis, while $a_y = \sqrt{10}$ has been set to create a uniform velocity along this direction. The optimized shape is shown in Figure 24(b). The convergence diagrams for the compliance and the volume are shown in Figure 25.

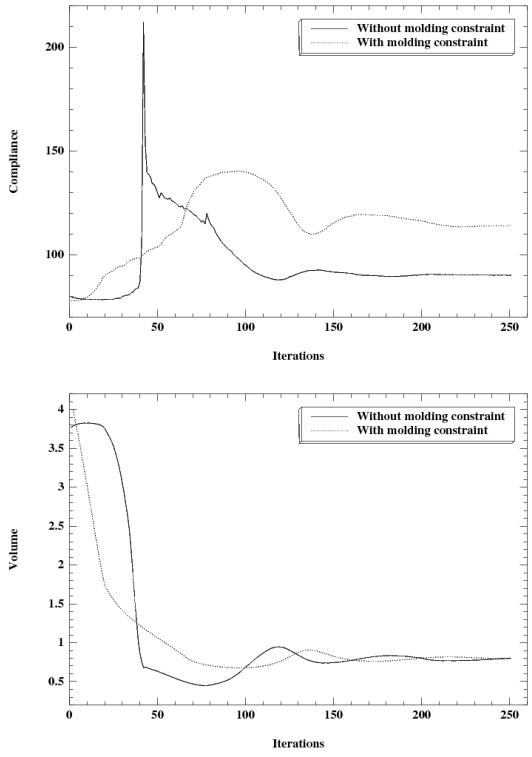

Fig. 15 Compliance (top) and volume (bottom) convergence diagrams for the results in Figures 9(bottom) and 14.

Acknowledgements The authors acknowledge fruitful discussions and helpful remarks from Marc Albertelli (Renault) and Charles Dapogny (Laboratoire Jean Kuntzmann, CNRS, Université de Grenoble). This work has been supported by the RODIN project (FUI AAP 13). G. Allaire is a member of the DEFI project at INRIA Saclay Ile-de-France.

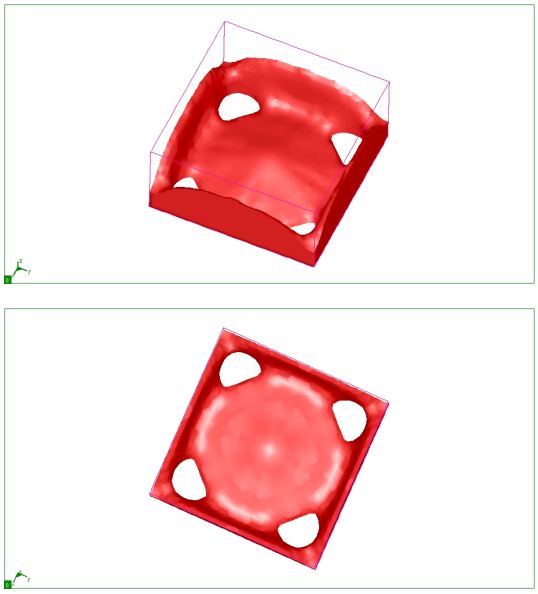

Fig. 16 Optimized shape for the optimization problem (27), with a maximum thickness constraint, setting $d = (0,0,1)$ as casting direction and using the molding direction condition (9).

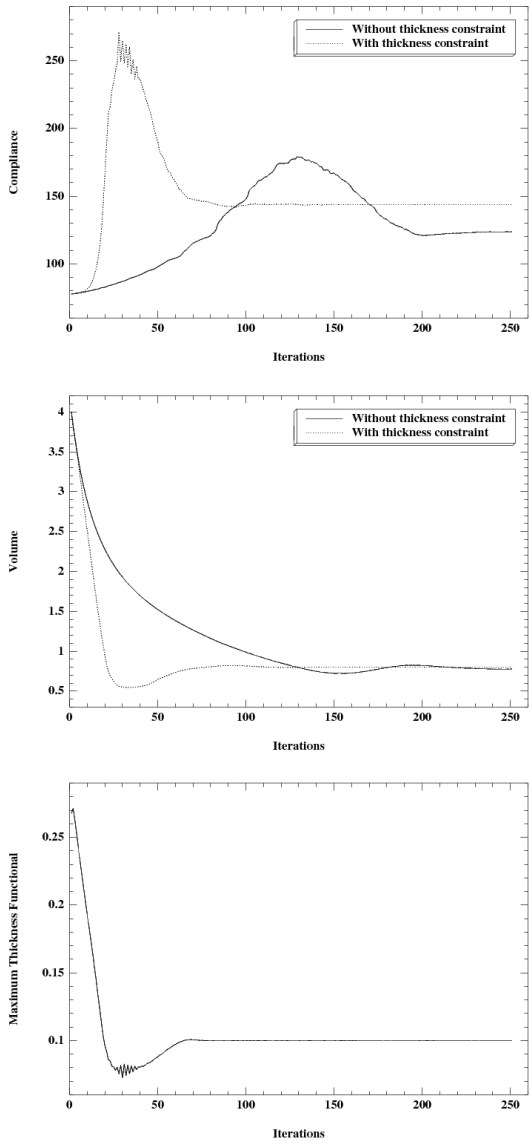

Fig. 17 Compliance (top) and volume (middle) convergence diagrams for the results in figures 10(bottom) and 16; convergence diagram for the maximum thickness functional (bottom) $P_{MaxT}(\Omega)$ for the optimized shape in Figure 16.

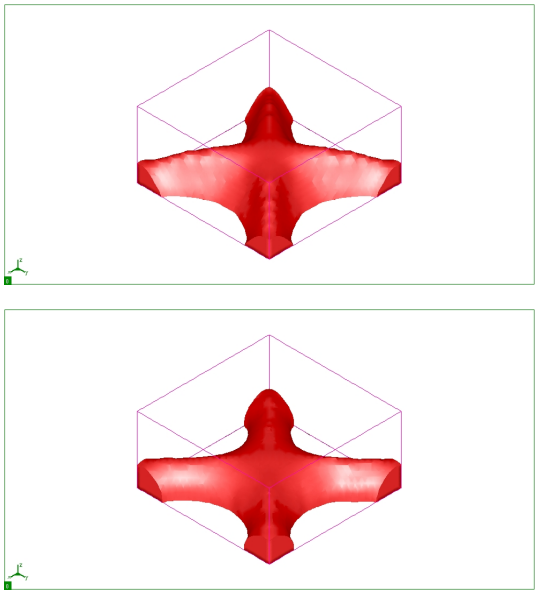

Fig. 18 Optimized shapes under: a molding constraint (top) and: a molding and minimum thickness constraint (bottom), with a predefined parting surface at $z = 0$.

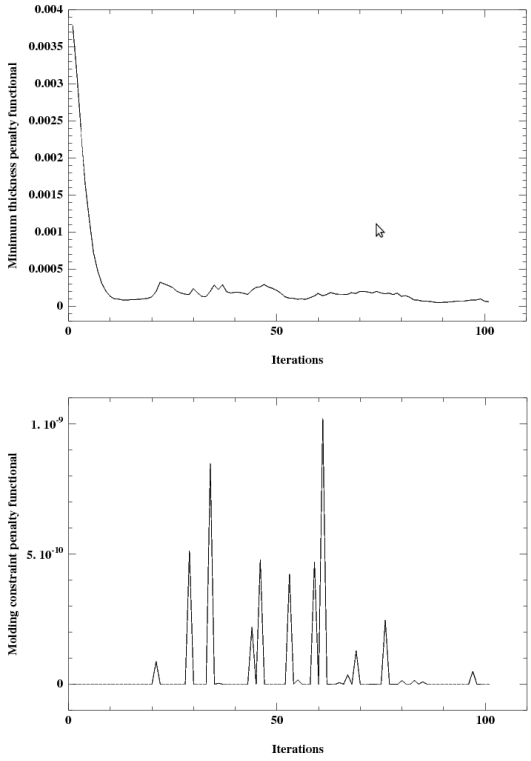

Fig. 19 Convergence diagrams for the penalty functionals: P_1 (top) and: P_2 (bottom), for the results of Figure (18)(bottom).

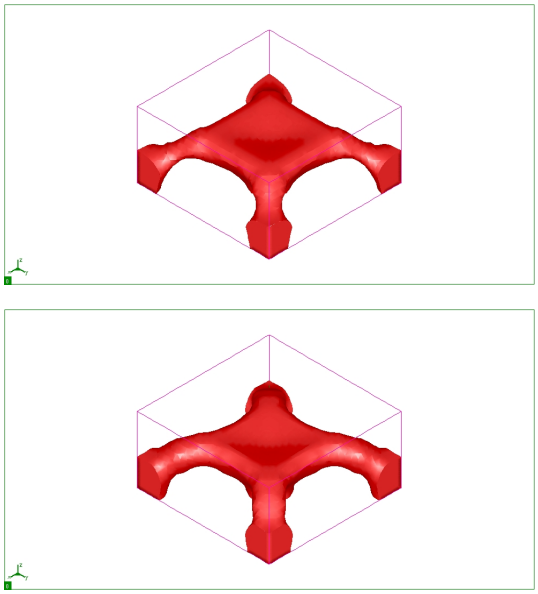

Fig. 20 Optimized shapes under: a molding constraint (top) and: a molding and minimum thickness constraint (bottom), without a predefined parting surface.

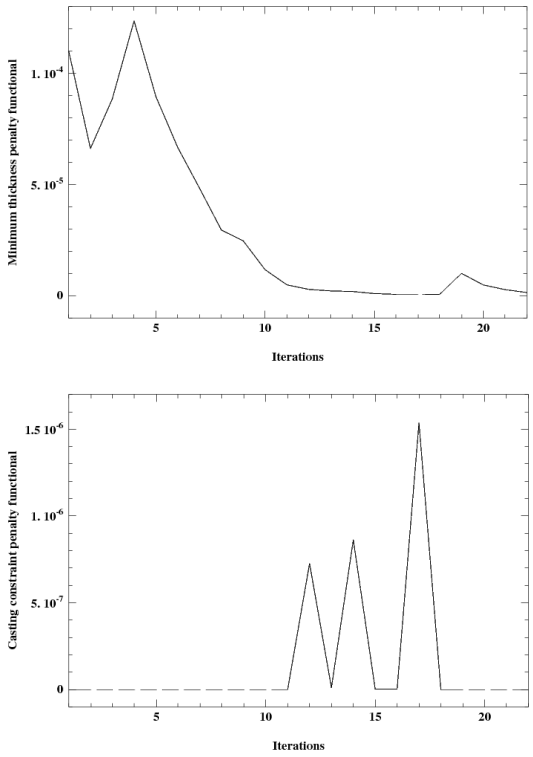

Fig. 21 Convergence diagrams for the penalty functionals: P_1 (top) and: P_2 (bottom), for the results of Figure (20)(bottom).

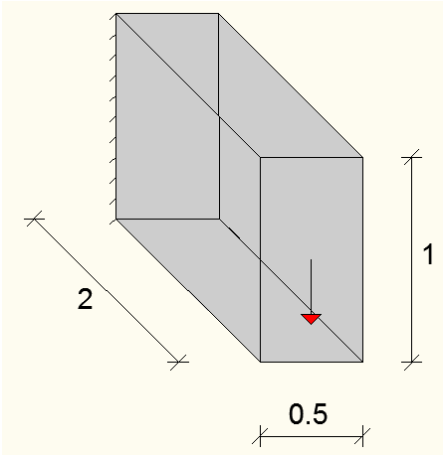

Fig. 22 Boundary conditions for the ”uniform cross-section” test case.

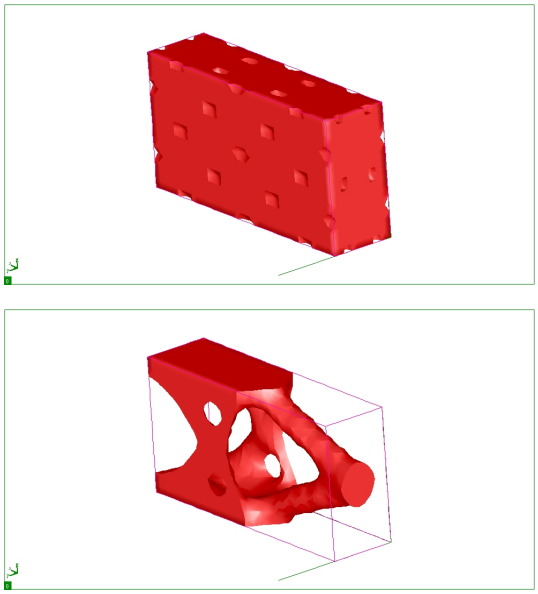

Fig. 23 Initialization (top) and optimized shape (bottom), without the "uniform cross-section" constraint.

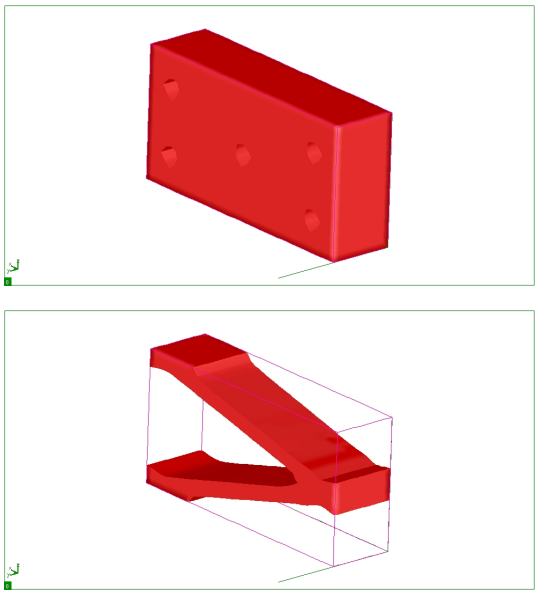

Fig. 24 Initialization (top) and optimized shape (bottom), with a "uniform cross-section" constraint.

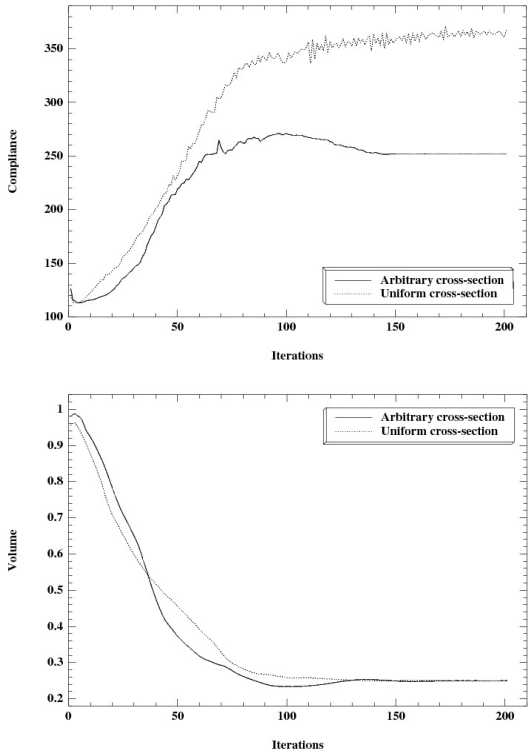

Fig. 25 Compliance (top) and volume (bottom) convergence diagrams for the results of figures 23 and 24.

References

1. H.K. Ahn, M. De Berg, P. Bose, S.W. Cheng, D. Halperin, J. Matoušek, and O. Schwarzkopf. Separating an object from its cast. *Computer-Aided Design*, 34(8):547–559, 2002.
2. G. Allaire. *Conception optimale de structures*, volume 58 of *Mathématiques & Applications*. Springer-Verlag, Berlin, 2007.
3. G. Allaire, E. Bonnetier, G. Francfort, and F. Jouve. Shape optimization by the homogenization method. *Numerische Mathematik*, 76(1):27–68, 1997.
4. G. Allaire, C. Dapogny, G. Delgado, and G. Michailidis. Mutli-phase structural optimization via a level-set method. *ESAIM: Control, Optimisation and Calculus of Variations, 20, pp 576-611*, 2014.
5. G. Allaire, C. Dapogny, and P. Frey. Topology and geometry optimization of elastic structures by exact deformation of simplicial mesh. *Comptes Rendus Mathématique*, 349(17):999–1003, 2011.
6. G. Allaire, C. Dapogny, and P. Frey. Shape optimization with a level set based mesh evolution method. *Comput. Methods Appl. Mech. Engrg.*, 282:22–53, 2014.
7. G. Allaire and F. Jouve. A level-set method for vibration and multiple loads structural optimization. *Computer methods in applied mechanics and engineering*, 194(30):3269–3290, 2005.
8. G. Allaire, F. Jouve, and G. Michailidis. Casting constraints in structural optimization via a level-set method. In *WCSMO-10, Orlando, Florida, USA*, 2013.
9. G. Allaire, F. Jouve, and G. Michailidis. Thickness control in structural optimization via a level set method. *(to appear in SMO), HAL preprint: hal-00985000v1*, 2014.
10. G. Allaire, F. Jouve, and A.-M. Toader. A level-set method for shape optimization. C. R. Acad. Sci. Paris, Série I, 334:1125–1130, 2002.
11. G. Allaire, F. Jouve, and A.-M. Toader. Structural optimization using sensitivity analysis and a level-set method. *Journal of computational physics*, 194(1):363–393, 2004.
12. G. Allaire, F. Jouve, and N. Van Goethem. Damage and fracture evolution in brittle materials by shape optimization methods. *Journal of Computational Physics*, 230(12):5010–5044, 2011.
13. G. Allaire and R.V. Kohn. Optimal design for minimum weight and compliance in plane stress using extremal microstructures. *European journal of mechanics. A. Solids*, 12(6):839–878, 1993.
14. M.P. Bendsøe. Optimal shape design as a material distribution problem. *Structural and Multidisciplinary Optimization*, 1(4):193–202, 1989.
15. M.P. Bendsøe and N. Kikuchi. Generating optimal topologies in structural design using a homogenization method. *Computer methods in applied mechanics and engineering*, 71(2):197–224, 1988.
16. M.P. Bendsoe and O. Sigmund. *Topology optimization: theory, methods and applications*. Springer, 2004.
17. L. Blank, H. Farshbaf-Shaker, H. Garcke, and V. Styles. Relating phase field and sharp interface approaches to structural topology optimization. *ESAIM Control Optim. Calc. Var.*, 20(4):1025–1058, 2014.
18. B. Bourdin and A. Chambolle. Design-dependent loads in topology optimization. *ESAIM Control Optim. Calc. Var.*, 9:19–48, 2003.
19. J. Campbell. *Castings, 1991*. Butterworth Heinemann, Great Britain, 1964.
20. F. de Gournay. Velocity extension for the level-set method and multiple eigenvalues in shape optimization. *SIAM journal on control and optimization*, 45(1):343–367, 2006.
21. F. de Gournay, G. Allaire, and F. Jouve. Shape and topology optimization of the robust compliance via the level set method. *ESAIM: Control, Optimisation and Calculus of Variations*, 14(01):43–70, 2008.
22. M.W. Fu, A.Y.C. Nee, and J.Y.H. Fuh. The application of surface visibility and moldability to parting line generation. *Computer-Aided Design*, 34(6):469–480, 2002.

23. L. Harzheim and G. Graf. Optimization of engineering components with the sko method. *SAE Technical Paper*, 951104, 1995.
24. L. Harzheim and G. Graf. Topshape: An attempt to create design proposals including manufacturing constraints. *International journal of vehicle design*, 28(4):389–409, 2002.
25. L. Harzheim and G. Graf. A review of optimization of cast parts using topology optimization: Ii - topology optimization without manufacturing constraints. *Structural and multidisciplinary optimization*, 30(5):491–497, 2005.
26. L. Harzheim and G. Graf. A review of optimization of cast parts using topology optimization: I - topology optimization with manufacturing constraints. *Structural and multidisciplinary optimization*, 31(5):388–399, 2006.
27. A. Henrot and M. Pierre. *Variation et optimisation de formes: une analyse géométrique*, volume 48. Springer, 2005.
28. A. Laadhari, C. Misbah, and P. Saramito. On the equilibrium equation for a generalized biological membrane energy by using a shape optimization approach. *Physica D: Nonlinear Phenomena*, 239(16):1567–1572, 2010.
29. J.P. Leiva, B.C. Watson, and I. Kosaka. An analytical directional growth topology parameterization to enforce manufacturing requirements. In *Proc. of 45th AIAA/ASME/ASCE/AHS/ASC Structures, Structural Dynamics, and Material Conference, Palm Springs, CA*, 2004.
30. RW Lewis, MT Manzari, and DT Gethin. Thermal optimisation in the sand casting process. *Engineering Computations*, 18(3/4):392–417, 2001.
31. C. Mattheck. Design and growth rules for biological structures and their application to engineering. *Fatigue & Fracture of Engineering Materials & Structures*, 13(5):535–550, 1990.
32. G. Michailidis. *Manufacturing Constraints and Multi-Phase Shape and Topology Optimization via a Level-Set Method*. PhD thesis, Ecole Polytechnique X, 2014, available at: http://pastel.archives-ouvertes.fr/pastel-00937306.
33. B. Mohammadi and O. Pironneau. *Applied shape optimization for fluids*, volume 28. Oxford University Press Oxford, 2001.
34. F. Murat and J. Simon. Etude de problèmes d'optimal design. *Optimization Techniques Modeling and Optimization in the Service of Man Part 2*, pages 54–62, 1976.
35. S.J. Osher and F. Santosa. Level set methods for optimization problems involving geometry and constraints: I. frequencies of a two-density inhomogeneous drum. *Journal of Computational Physics*, 171(1):272–288, 2001.
36. S.J. Osher and J.A. Sethian. Fronts propagating with curvature-dependent speed: algorithms based on hamilton-jacobi formulations. *Journal of computational physics*, 79(1):12–49, 1988.
37. J.A. Sethian. *Level set methods and fast marching methods: evolving interfaces in computational geometry, fluid mechanics, computer vision, and materials science*. Cambridge university press, 1999.
38. J.A. Sethian and A. Wiegmann. Structural boundary design via level set and immersed interface methods. *Journal of computational physics*, 163(2):489–528, 2000.
39. J. Sokołowski and J.-P. Zolésio. *Introduction to shape optimization*. Springer-Verlag, Berlin, 1992.
40. SYSTUS2014, SYSWELD2014, User's manual, SYSTUS International, 2014.
41. A. Takezawa, S. Nishiwaki, and M. Kitamura. Shape and topology optimization based on the phase field method and sensitivity analysis. *Journal of Computational Physics*, 229(7):2697–2718, 2010.
42. R. Tavakoli and P. Davami. Optimal riser design in sand casting process by topology optimization with simp method i: Poisson approximation of nonlinear heat transfer equation. *Structural and Multidisciplinary Optimization*, 36(2):193–202, 2008.
43. D.A. Tortorelli, M.M. Tiller, and J.A. Dantzig. Optimal design of nonlinear parabolic systems. part i: Fixed spatial domain with applications to process optimization. *Computer methods in applied mechanics and engineering*, 113(1):141–155, 1994.
44. X. Wang, M.Y. Wang, and D. Guo. Structural shape and topology optimization in a level-set-based framework of region representation. *Structural and Multidisciplinary Optimization*, 27(1):1–19, 2004.

45. Q. Xia, T. Shi, S. Liu, and M.Y. Wang. A level set solution to the stress-based structural shape and topology optimization. *Computers and Structures*, 9091(0):55 – 64, 2012.
46. Q. Xia, T. Shi, M.Y. Wang, and S. Liu. A level set based method for the optimization of cast part. *Structural and Multidisciplinary Optimization*, 41(5):735–747, 2010.
47. Q. Xia, T. Shi, M.Y. Wang, and S. Liu. Simultaneous optimization of cast part and parting direction using level set method. *Structural and Multidisciplinary Optimization*, 44(6):751–759, 2011.
48. T. Yamada, K. Izui, S. Nishiwaki, and A. Takezawa. A topology optimization method based on the level set method incorporating a fictitious interface energy. *Computer Methods in Applied Mechanics and Engineering*, 199(45):2876–2891, 2010.
49. M. Zhou and G.I.N. Rozvany. The coc algorithm, part ii: topological, geometrical and generalized shape optimization. *Computer Methods in Applied Mechanics and Engineering*, 89(1):309–336, 1991.
50. M. Zhou, Y.K. Shyy, and H.L. Thomas. Topology optimization with manufacturing constraints. In *Proceedings of the 4th World Congress of Structural and Multidisciplinary Optimization*, 2001.
51. S. Zhou and M.Y. Wang. Multimaterial structural topology optimization with a generalized cahn–hilliard model of multiphase transition. *Structural and Multidisciplinary Optimization*, 33(2):89–111, 2007.